Research Article Vol. 14, No. 11 / 1 Nov 2024 / Optical Materials Express 2527
Optical Materials EXPRESS

Astigmatic thermal lensing due to surface bulging in Yb:KYW laser crystals

MALTE BIERINGER,[1] JOHANNES WEITENBERG,[1,2] THOMAS UDEM,[1,3] AND AKIRA OZAWA[1,*]

[1]Max-Planck-Institut für Quantenoptik, Hans-Kopfermann-Straße 1, 85748 Garching, Germany
[2]Fraunhofer-Institut für Lasertechnik ILT, Steinbachstraße 15, 52074 Aachen, Germany
[3]Fakultät für Physik, Ludwig-Maximilians-Universität München, Schellingstraße 4, 80799 Munich, Germany
*akira.ozawa@mpq.mpg.de

Abstract: One of the sources of thermal lensing in crystals is surface bulging that results from an inhomogeneous temperature distribution. We investigate a thermal lens caused by surface bulging in an end-pumped Yb:KYW crystal, which serves as a gain medium in lasers and optical amplifiers. The surface profile of the pumped crystal is measured using a Fizeau-type interferometer and compared with a numerical simulation using a finite element method. The study reveals that due to anisotropic thermal expansion, the surface shape of the Yb:KYW crystal is anisotropic and the profile of the expansion is transversely displaced with respect to the pump beam profile which generates the temperature distribution. The observed surface bulging gives rise to aberrations and deflection of the transmitted beam. It was found that the surface bulging introduces astigmatism that is significantly larger than previously estimated [Appl. Opt. **56**, 3857 (2017)]. Our results allow the evaluation of the bulging contribution with improved accuracy. We show that these effects can be significant in certain designs of amplifiers and lasers.

1. Introduction

When a high-power light beam propagates through an absorbing medium, the spatial distribution of the temperature in the medium changes due to the heat deposited by the beam. The inhomogeneous temperature distribution affects the refractive index directly via its temperature dependence and indirectly via thermal expansion which additionally induces stress and strain. The change of refractive index introduces a phase shift that depends on the distance of a given ray from the optical axis. The effects can be approximated as a focusing or defocusing lens with aberrations. This is referred to as thermal lensing. Among other unfavorable temperature-induced effects, such as depolarization due to stress-induced birefringence and thermal fracture of the gain medium, thermal lensing is known to be one of the most important limitations in scaling the output power of lasers and optical amplifiers [1]. To mitigate this effect and allow power-scaling beyond few 10 W, three different schemes are commonly employed: The Innoslab design uses heat flow in one transverse direction and a large aspect ratio of the pumped area to reduce thermal lensing and aberrations compared to a rod with a round pump area and radial heat flow [2,3]. In thin-disk lasers and amplifiers the heat flow and thermal gradient is in the direction of the beam propagation, thereby mainly eliminating the focusing effect on the beam [4]. In fiber lasers and amplifiers the strong thermal lens does not affect the beam, as it is propagating in a (single-mode) waveguide. A gain medium in an end-pumped rod geometry can still be used for lasers and amplifiers with modest output power. The rod is cylindrical or cuboidal in shape, with the cylinder axis coinciding with the beam propagation axis. For example, a laser based on a rod-shaped Yb:KGW crystal has been built in an end-pumped configuration [5], i.e. pump and laser beam propagate in the same direction. An average output power of 12 W at 1044 nm using 25 W pump radiation from a diode laser was demonstrated [5]. Yb-doped gain materials are widely used in

#530949 https://doi.org/10.1364/OME.530949
Journal © 2024 Received 22 May 2024; revised 12 Sep 2024; accepted 12 Sep 2024; published 7 Oct 2024

Optical Materials EXPRESS

near-infrared optical amplifiers due to their small quantum defect, high pump quantum efficiency, convenient pump wavelength where high-power laser diodes are available and simple electronic structure with no upper-state absorption or quenching. Furthermore they support fs-pulses. There are several crystals commonly used to host Yb^{3+} ions, including yttrium aluminum garnet (YAG), yttrium lithium fluoride (YLF), yttrium orthovanadate (YVO), potassium gadolinium tungstate (KGW), and potassium yttrium tungstate (KYW). The latter two materials support shorter pulses compared to Yb:YAG. Due to the low crystal symmetry of the latter two materials, it is necessary to include the full anisotropic thermal expansion and photoelastic tensors to model the thermal lensing effects. Previously, the bulging contribution was estimated by a simplified theoretical model of the surface deformation ignoring the off-diagonal entries of the thermal expansion matrix [6]. In this work we present an experimental observation and a detailed numerical study of thermally induced surface bulging in a KYW crystal. The results allow a direct and more accurate evaluation of the bulging contributions. This is important for estimating the photoelastic and thermo-optical contributions of the thermal lens [7]. We show that due to anisotropic thermal expansion, surface bulging introduces an anisotropic lensing effect with aberrations and deflection in the transmitted beam.

2. Theoretical modeling of the thermal lensing effect

The effect of thermal lensing has been modeled for various crystal shapes and pump geometries. One of the simplest setups is a rod crystal with a (partially) end-pumped geometry, where partially end-pumped means that not the entire crystal volume is optically pumped. We assume that the temperature distribution in the gain medium is constant over time, which is often the case when using cw or high repetition rate pump sources. The temperature distribution inside the rod can then be obtained by solving the steady-state heat equation under the following assumptions [8,9]: the cooling geometry and the pump profile are axially symmetric and the thermal conductivity κ is reduced to a scalar quantity. In the case of weak anisotropy, the thermal conductivity can be approximated by its mean value. Furthermore, it is assumed that the material parameters (such as thermal expansion and thermal conductivity) do not change within the considered temperature range. As a boundary condition, it is assumed that the temperature at the surfaces of the rod in contact with the heat sink is kept constant. The derivation that we present here assumes a top-hat shaped pump beam with constant pump radius w_P along the rod length L. It can be adapted to Gaussian beams (or other beam shapes) in a straightforward fashion [10].

Inside the pumped volume the integrated temperature of the rod $\langle T(r)\rangle$ decreases quadratically with r [9]:

$$\langle T(r) - T(0)\rangle = \int_0^L (T(r,z) - T(0,z))\,\mathrm{d}z = -\frac{\eta_\mathrm{h} P_\mathrm{abs} r^2}{4\pi\kappa w_\mathrm{P}^2}, \tag{1}$$

where η_h is the fractional heat load defined as a fraction of the absorbed pump power dissipated as heat and P_abs is the total absorbed pump power. We use the notation of [9], where angle brackets do not denote an average, but an integration over z: For any quantity $A(r,z)$ which depends on the radial coordinate r and axial coordinate z we define $\langle A(r)\rangle = \int_0^L A(r,z)\mathrm{d}z$, which is essentially the average of $A(r,z)$ over the length L, but without normalization by L. Note that the integrated quantity $\langle A(r)\rangle$ no longer has z as an argument, and that $\langle A(r)\rangle$ has the dimension of $A(r,z)$ times length.

The refractive index bears the index j to denote its possible dependence on polarization, where light with polarization $E \parallel j$ is subject to the refractive index n_j. It can be expanded to first order around the constant temperature without pumping T_0 and zero strain $\vec{\varepsilon} = 0$:

$$n_j(T,\vec{\varepsilon}) = n_{0,j} + \left(\frac{\partial n_j}{\partial T}\right)_{\vec{\varepsilon}} (T(r,z) - T_0) + \sum_{i=x,y,z} \left(\frac{\partial n_j}{\partial \varepsilon_i}\right)_T \varepsilon_i(r,z). \tag{2}$$

Optical Materials EXPRESS

The strain vector $\vec{\varepsilon}$ contains three components $i = x, y, z$. Here we write $n_{0,j} = n_j(T = T_0, \vec{\varepsilon} = 0)$, and $\left(\partial n_j/\partial T\right)_{\vec{\varepsilon}}$ denotes the partial derivative of the refractive index with respect to temperature taken at constant strain, and $\left(\partial n_j/\partial \varepsilon_i\right)_T$ denotes the partial derivative with respect to the i–th component of the strain vector taken at constant temperature. By integrating $n_j(T, \vec{\varepsilon}) - n_{0,j}$ along the crystal length under thermal expansion, the optical path length difference $\delta_j(r)$ between the pumped and unpumped crystal can be written as [9]:

$$\delta_j(r) = \left(\frac{\partial n_j}{\partial T}\right)_{\vec{\varepsilon}} \langle T(r) - T_0\rangle + \sum_{i=x,y,z} \left(\frac{\partial n_j}{\partial \varepsilon_i}\right)_T \langle \varepsilon_i(r)\rangle + (n_{0,j} - 1)\Delta L(r), \tag{3}$$

where $\Delta L(r)$ is the thermal expansion of the rod along the pump axis at radius r.

The first term of Eq. (3) stands for the temperature dependence of the refractive index (thermo-optic effect) which we write using the thermo-optic coefficient $\left(\partial n_j/\partial T\right)_{\vec{\varepsilon}} = \chi_{\mathrm{T},j}$ [9]. It does not depend on polarization j in non-birefringent crystals because the refractive index is isotropic. In previous works [7,11], the thermo-optic effect has been modeled using the coefficient $\mathrm{d}n/\mathrm{d}T$. However, work by Chénais et al. [9] pointed out that in general $\mathrm{d}n_j/\mathrm{d}T \neq (\partial n_j/\partial T)_{\vec{\varepsilon}}$ and the difference can be substantial. Direct measurement of $\left(\partial n_j/\partial T\right)_{\vec{\varepsilon}}$ is challenging, because the photoelastic effect, i.e. the second term in Eq. (3) is always present (see below). In this work, we employ the the definition $\left(\partial n_j/\partial T\right)_{\vec{\varepsilon}} = \chi_{\mathrm{T},j}$ in the following discussions.

The second term in Eq. (3) is the photoelastic effect. It describes the variation of the material's polarizability associated with the interatomic distance change due to thermal expansion. The photoelastic effect can depend on light polarization even in isotropic crystals (stress birefringence). Applying Hooke's law and assuming plane stress, i.e. stress along z–direction (σ_z) is zero, [9] or plane strain ($\varepsilon_z = 0$) [8] the second term in (3) can be summarized by introducing the thermo–optic coefficient related to the photoelastic effect $\chi_{\mathrm{PE},j}$, short "photoelastic coefficient". It is used to rewrite the second term of Eq. (3) in terms of integrated temperature $\langle T(r)\rangle$:

$$\sum_{i=x,y,z} \left(\frac{\partial n_j}{\partial \varepsilon_i}\right)_T \langle \varepsilon_i(r)\rangle = \chi_{\mathrm{PE},j}\langle T(r) - T_0\rangle. \tag{4}$$

An analytical expression for $\chi_{\mathrm{PE},j}$ can be obtained from the thermal expansion matrix and elasto-optical tensor for isotropic gain medium and axial pump geometry [8,9]. In a general anisotropic material, the strain does not only depend on r, but can also depend on the azimuthal coordinate θ. In consequence, the photoelastic coefficient is not only polarization dependent, but also astigmatic.

The last term in Eq. (3) is the surface bulging effect, where the curved surfaces of the heated crystal act as a lens. By introducing another thermo-optic coefficient for the surface bulging contribution, short "bulging coefficient" χ_{bulg}, the elongation $\Delta L(r)$ of the crystal can be rewritten in terms of integrated temperature: $(n_0 - 1)\Delta L(r) = \chi_{\mathrm{bulg}}\langle T(r) - T_0\rangle$ [8,9]. In [9], Chénais and co-authors describe a simple model of $\chi_{\mathrm{bulg},\infty} = (n_0 - 1)(1 + \nu)\alpha_{\mathrm{T}}$ for an isotropic material, where ν is the Poisson ratio and α_{T} is the thermal expansion coefficient. The model is based on the assumption that the entire crystal length contributes to thermal expansion and there is no stress along the axial direction ($\sigma_z = 0$). On the other hand, if the pump radius w_{P} is significantly smaller than the rod length L, one expects the surface bulging to be smaller than given by this simple model. This is because only the parts close to the crystal surfaces contribute to the expansion, and the internal bulk is prevented from expanding by internal stresses. A model that includes this effect is proposed by Koechner [8]:

$$\chi_{\mathrm{bulg}} = (n_0 - 1)\alpha_{\mathrm{T}}(2l_0/L), \tag{5}$$

where l_0 is the length of the end section of the rod over which the expansion occurs. According to [8], l_0 is approximately given by w_{P}. The crossover from a constant $\chi_{\mathrm{bulg},\infty}$ to the w_{P} dependent

Optical Materials EXPRESS

expression (5) is expected to occur when the pump diameter is larger than the crystal length, namely $w_P^* = 2w_P/L > 1$. The surface bulging effect is symmetric in isotropic crystals in axially symmetric geometries, i.e., an axially symmetric beam propagating through a medium with rotationally symmetric crystal structure. This includes isotropic crystals, but also for example tetragonal crystals if the pump propagation axis coincides with the crystallographic c–axis [12]. The reason for this is that the temperature distribution is axially symmetric and the resulting thermal expansion maintains this symmetry. For crystals with a low symmetry group, such as Yb:KYW, the analytical descriptions above cannot be applied and one has to rely on numerical and experimental studies.

Using Eq. (1), Eq. (3) and the coefficients introduced above, the dioptric power D of the thermal lens can be expressed as [9]

$$D = \frac{2}{r^2}\left(\delta(0) - \delta(r)\right) = \frac{\eta_h P_{abs}}{2\pi w_P^2 \kappa}\left(\chi_T + \chi_{PE} + \chi_{bulg}\right). \tag{6}$$

In a general anisotropic material, $\chi_T + \chi_{PE}$ can be astigmatic and polarization dependent. χ_{bulg} can also be astigmatic. Equation (6) only holds for isotropic thermal conductivity. If κ is anisotropic, one should not calculate a different dioptric power for each eigenvalue of κ because this neglects the azimuthal heat flow. Our simulation shows that the temperature profile is weakly dependent on the azimuthal coordinate θ even when using the anisotropic thermal conductivity matrix, and it is a better approximation to replace κ by the mean of its eigenvalues. Equation (6) was derived for a top-hat pump beam. It coincides to lowest order in r with the expression for a Gaussian pump beam after multiplying the right hand side of Eq. (6) by a factor of 2 [10].

For Yb:KYW crystals, Loiko and co-authors [13] reported values for $\mathrm{d}n/\mathrm{d}T$ between −7.6 and -14.6×10^{-6} K^{-1} for wavelength of $\lambda = 1064$ nm (depending on polarization and Yb doping). Note that $\mathrm{d}n/\mathrm{d}T$ has negative sign, but that the measurement is performed under constant stress and therefore the thermo-optic coefficient measured in this reference does not correspond to χ_T in (6).

The photoelastic coefficient (χ_{PE}) was measured to be -1.3×10^{-6} K^{-1} (mg–plane) and -2.9×10^{-6} K^{-1} (pg–plane) for light with $k \parallel N_g$ and $E \parallel N_m$. For the polarization $E \parallel Np$ the measured χ_{PE} is 0.4×10^{-6} K^{-1} and 2.0×10^{-6} K^{-1} for the mg– and pg–planes, respectively [7]. These values were determined by measuring the overall thermo-optic coefficient $\chi = \chi_T + \chi_{PE} + \chi_{bulg}$ and subtracting the previously measured χ_T [13] and χ_{bulg} [6]. This indirect process of determining χ_{PE} has significant uncertainty because of the limited accuracy in the experimental determination of χ_T.

The evaluation of the bulging coefficient (χ_{bulg}) is not straightforward for Yb:KYW, because the thermal expansion is anisotropic and has to be described by a matrix which is not even diagonal in the eigenframe of the refractive index ellipsoid [6]. The surface bulging can be simulated for a Yb:KYW crystal using the experimentally measured thermal conductivity [14], the elasticity matrix [15] and the thermal expansion matrix [6]. The thermal expansion matrix was measured for pure KYW (i.e. 0% atomic (at.) Yb doping) and pure KYbW (i.e. 100% at. Yb doping, all of the Y ions are replaced by Yb ions) crystals, respectively [6]. We assumed a linear dependence of the thermal expansion on the Yb doping and obtained the expansion matrix of the Yb:KYW crystal with 10% Yb concentration as

$$\alpha_T = \begin{pmatrix} 10.8 & 0 & -5.8 \\ 0 & 2.0 & 0 \\ -5.8 & 0 & 17.0 \end{pmatrix} \times 10^{-6}\ \mathrm{K}^{-1}. \tag{7}$$

The matrix is defined in the eigenframe of the refractive index ellipsoid where $x = N_m$, $y = N_p$ and $z = N_g$. Under end-pumped geometries, the thermal lensing effect due to surface bulging

Optical Materials EXPRESS

is expected to be significant for Yb:KYW crystal compared with Yb:YAG. This is because the largest eigenvalue of the thermal expansion matrix ranges from $(21-15)\times10^{-6}$ K^{-1} depending on the Yb doping [6], which is three times larger than the thermal expansion of the YAG crystal. In addition, asymmetric thermal lensing and aberrations can be introduced due to the non-diagonal thermal expansion of Yb:KYW in the eigenframe of the refractive index ellipsoid and its low-symmetry crystal structure.

Asymmetric thermal lensing due to surface bulging induced by non-diagonal thermal expansion matrix has been studied analytically in Nd:YVO_4 [12]. Nd:YVO_4 is a tetragonal crystal and has only two different entries in its thermal expansion matrix. This causes the surface bulging contribution thermal lens to have two different dioptric powers, i.e. astigmatism which can be described by two different values of the bulging coefficient χ_{bulg}. The planes of maximum and minimum dioptric power will be referred to as meridional and sagittal plane for the rest of this paper. In this work the astigmatism will be quantified by the normalized difference of the dioptric powers in these planes. The astigmatism caused by the surface bulging is expected to be between 8 and 10% [12]. The anisotropy of the thermal expansion matrix in YVO_4 is (1:1:3.8) [16] and considerably smaller than that of KYW (1:3.6:10.5) [6]. Here the anisotropy is defined as the ratio of the eigenvalues of the thermal expansion matrix. The magnitude of many entries in the thermal expansion matrix is larger in KYW than in YVO_4, so the thermal lensing due to surface bulging is larger in KYW.

Yb-doped yttrium aluminum garnet (Yb:YAG) is another widely used gain material. The thermo-optic coefficients of Yb:YAG have also been intensively studied. The measured overall thermo-optic coefficient is $\chi_T+\chi_{PE}+\chi_{bulg}=10\times10^{-6}$ K^{-1} [9]. The surface bulging contribution is $\chi_{bulg}=(n_0-1)\alpha_T=4.2\times10^{-6}$ K^{-1}, assuming $\alpha_T=5.1\times10^{-6}$ at 50 °C [17], and $n=1.82$ [8]. It was shown that in side-cooled rods the surface bulging can cause more than 30% of the overall thermal lens [18].

Three different effects, namely the thermo-optical effect χ_T, the photoelastic effect χ_{PE}, and the surface bulging χ_{bulg}, contribute to thermal lensing. In the experimental measurement on the Yb:KYW crystal by [7], only the sum of these can be obtained. Since it is difficult to accurately estimate the χ_T and χ_{PE} coefficients either experimentally or analytically, an evaluation of χ_{bulg} is important to understand the different contributions of thermal lensing in Yb:KYW. In addition, understanding the possible aberrations and asymmetric thermal lensing due to non-diagonal thermal expansion matrix entries and low-symmetry crystal structures helps to design Yb:KYW lasers and amplifiers with good beam quality.

3. Experimental and numerical evaluation of the surface bulging

3.1. Experiment

The surface bulging of the pumped KYW crystal was measured using a Fizeau type interferometer. The schematic of the setup is shown in Fig. 1. We used a N_g–cut 10% at. doped Yb:KYW crystal with dimensions of $4(N_m)\times3(N_p)\times1(N_g)$ mm^3. The crystal was clamped between 1 mm thick indium layers and the S1 and S2 surfaces (see Fig. 2) were thermally and mechanically connected to a water-cooled copper mount. The crystal had an anti-reflection (AR) coating on both sides for 935 nm. A multimode fiber-coupled diode laser at 935 nm and maximum power of 7.5 W was focused in the crystal using a lens (f = 150 mm). Since the output facet of the pump–fiber was imaged onto the crystal, the pump beam had flat-top profile at the focus and its radius was measured to be 160 µm. A highly reflective coating of 532 nm was applied to the back surface (R1). A significant portion of the transmitted pump power (about 2 W) was dumped after passing through a near-infrared (NIR) transmissive mirror M1. The residual pump beam reflected from mirror M1 was blocked by a 532 nm bandpass filter (F1). The probe beam at 532 nm was sent into the setup and the reflection from the back surface of the crystal (R1) and the beam from the

Optical Materials EXPRESS

partially reflecting flat reference mirror (R2) were spatially overlapped. The crystal surface was imaged on a CMOS camera to observe the interference pattern between these beams.

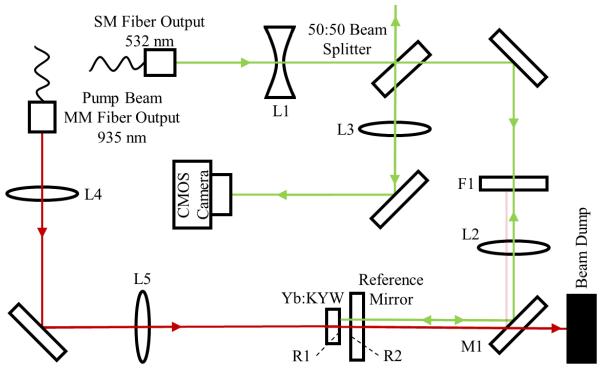

Fig. 1. The schematic of the Fizeau type interferometer setup for measuring the surface bulging effect. A single-mode fiber coupled green beam at 532 nm is sent into the interferometer that consists of a Yb:KYW crystal and a flat reference mirror. The Yb:KYW crystal is illuminated by a pump beam at 935 nm delivered by a multi-mode fiber. The crystal surfaces have an anti-reflection coating at the pump wavelength. The focal radius of the pump beam at the crystal is 160 μm. The back-surface (R1) of the crystal, which is under investigation, has a dielectric coating that reflects at 532 nm and transmits the pump radiation. The surface R2 of the reference flat mirror has transmission of 50% in the visible range, while the other surface is AR coated in the visible range. The R2 surface has about 70% of transmission for the pump wavelength (935 nm). The green beam reflected from the crystal surface (R1) spatially overlaps with the beam reflected from the partially transmissive reference mirror (R2). The both beams are sent to a camera and the interference images between them are recorded. L1, L2 and L3 are lenses to shape the green beam from the fiber and to image the crystal surface onto the camera detector plane. An optical bandpass filter (F1) centered at 532 nm is installed to block the residual pump beam and flourescence from the crystal. L4 and L5 are lenses to collimate and focus the pump beam.

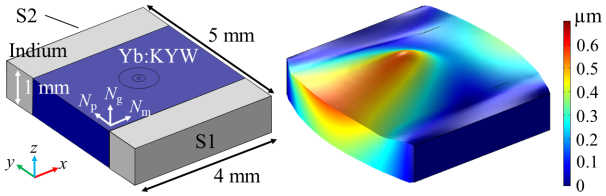

Fig. 2. 3D view of the simulated crystal without (left) and with heating by the pump beam (right). The crystal surface is in the *xy*–plane and the beam propagates along the *z*–axis. The optical axes N_m, N_p, N_g are aligned with the *x*–, *y*–, and *z*– axes, respectively. In the left image, the Yb:KYW crystal is shown in blue. The indium layers (gray) are for thermal connection to the heat sink (not shown). In the simulation, the surfaces S1 and S2 are kept at a constant position and temperature. The simulation was performed with the COMSOL Multiphysics software [19]. In the right image, the displacement of the crystal surfaces is exaggerated by a factor of 1500. The colors show the absolute value of the displacement vector. Note that this is different from Fig. 4 which only shows the *z*-component of the displacement vector.

The examples of measured interferograms are shown in Fig. 3. The reference mirror was tilted along one of the crystal axes to obtain interference fringes with convenient spacing for the

Optical Materials EXPRESS

data analysis. The resulting images Fig. 3(a,b) were smoothed by applying a convolution with Gaussian kernel. The $1/e^2$ radius was chosen to be 0.4 pixel in the x–direction and 1.5 pixel in the y–direction. The profile of the surface R1 was reconstructed from the fringe positions. By subtracting the height profile measured without pumping, the profile of the surface bulging due to heating by the pump beam was extracted. The result is shown in Fig. 4(a). The spatial offsets in x–, y– and z–direction were adjusted to best fit to the simulation data.

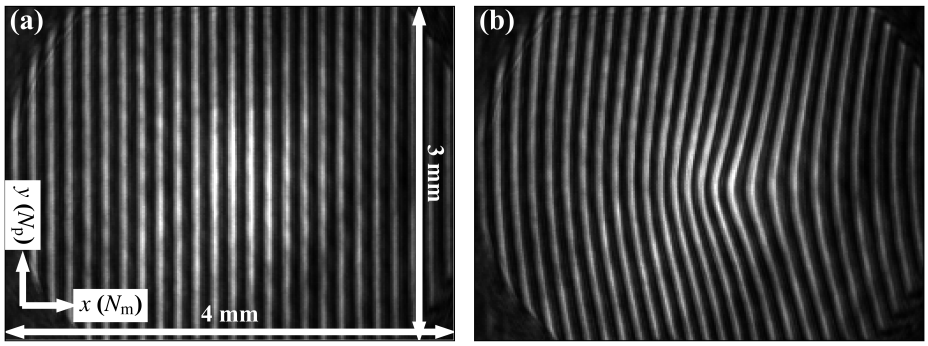

Fig. 3. Examples of measured interferograms for the pump off (a) and on (b) with a pump average power of 7.66 W. The crystal axes and scales shown in (a) apply to (b) as well.

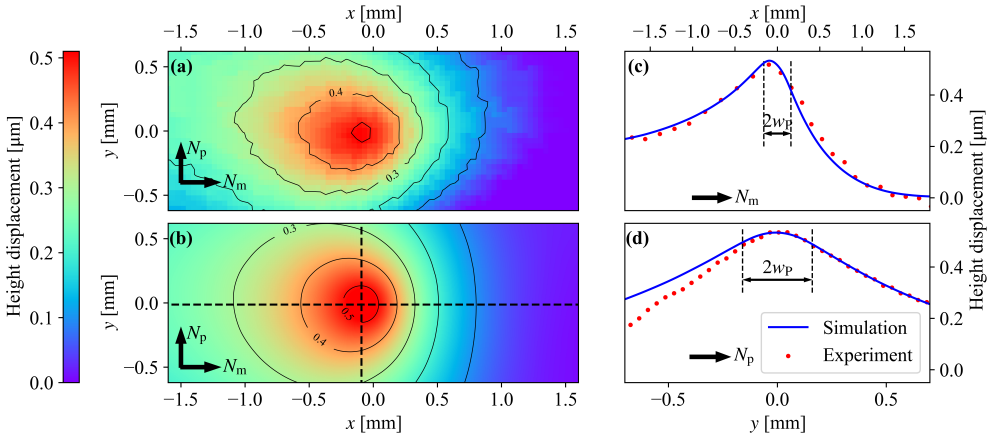

Fig. 4. Comparison of numerical simulation of surface bulging with measurement. All plots show the height displacement (z–direction) in µm. (a) Measured height displacement, (b) height displacement obtained by numerical simulation, (c) cut in x–direction along the horizontal black dashed line in (b). (d) cut in y–direction along vertical black dashed line in (b). In both (c) and (d), the red dots and blue lines correspond to the measured and simulated height displacements, respectively. For the orientation of the coordinate axes, see Fig. 2. The pump beam is sent along z–axis at $x = y = 0$ in the simulation. The simulation and the measurement are performed with the incident pump power $P_0 = 7.66$ W, the pump beam radius $w_P = 160$ µm, the effective absorption coefficient $\alpha = 937$ m^{-1} (see main text) and a Yb doping of 10% at.

3.2. Numerical simulation

To investigate the surface bulging of a Yb:KYW crystal, a finite element numerical simulation was performed for a simple amplifier geometry with end-pumping. The numerical simulations

Optical Materials EXPRESS

were performed using the software package COMSOL Multiphysics [19]. We pick the x–axis to coincide with the optical N_m–axis, the y–axis with the N_p–axis, and the pump propagates in positive z–(N_g–) direction (see Fig. 2). The heat deposited by the pump beam is modeled by the following heat source:

$$q(x,y,z) = \frac{\eta_h P_0 \alpha}{\pi w_P^2} \exp(-\alpha z)\, \Theta\left(w_P^2 - x^2 - y^2\right), \tag{8}$$

where Θ is the Heaviside step function and P_0 is the incident pump power. The heat density (8) corresponds to a top-hat pump beam with neglected beam divergence. This corresponds to our experimental situation, because the facet of the multimode fiber is imaged directly inside the crystal and the Rayleigh length of the pump beam is longer than the crystal by a factor of 3. At surface R2 (see Fig. 1) 30% of the pump power that is transmitted through the crystal is backreflected into the crystal. This power is added to the heat source (8). We model absorption saturation by measuring the transmitted power P_1 and assigning the constant effective absorption coefficient $\alpha = \log(P_0/P_1)/L = 937\ \mathrm{m}^{-1}$. It is assumed that the power still decays exponentially $\sim \exp(-\alpha z)$, but with the effective absorption coefficient α from our measurement, which is a good approximation for a modest saturation. The maximum intensity is around one third of the saturation intensity. We model the heat source Eq. (8) to be as close as possible to our specific experimental parameters. However, Eq. (8) can be modified to model any given beam shape and absorption profile by replacing the Θ–function by its corresponding expression and $P_0\alpha \exp(-\alpha z) \to -\mathrm{d}P_P/\mathrm{d}z$ [9]. The derivative $\mathrm{d}P_P/\mathrm{d}z$ denotes the depletion of pump power in propagation direction.

The parameters and dimensions of the crystal for the simulation are set to be identical to the ones used in the measurement described in the previous section. We used the anisotropic thermal conductivity [14], elasticity matrix [15] and thermal expansion matrix (Eq. (7)). The fractional heat load is assumed to be $\eta_h = 10\%$. At surfaces S1 and S2 (see Fig. 2) the crystal is sandwiched between two layers of indium, each with a thickness of 1 mm. In the simulation, the surfaces S1 and S2 are set to a constant temperature of 16°C. In addition, the distance between S1 and S2 is fixed. A heat transfer coefficient of 1 $\mathrm{Wcm}^{-2}\mathrm{K}^{-1}$ is assumed between the Yb:KYW crystal and the indium [9]. All surfaces exposed to air are assumed to be thermally insulating. This is a good approximation because the heat transfer coefficient from the surfaces of the materials to the air is very small compared to the heat transfer to the indium. The structure is allowed to expand freely except for the S1 and S2 surfaces. The thermal expansion matrix is assumed to be constant over temperature. The variation of the matrix elements is at most 15-20% for the temperature range under consideration [20]. The mesh for the finite element simulation is generated adaptively: the element size is small in the vicinity of the heat source and increases accordingly with the distance from the center. The displacements of the surfaces due to thermal expansion are obtained from the simulation and shown in Figs. 2 and 4. Note that Fig. 2 shows the absolute value of the displacement vector while in Fig. 4 only the z-component is shown.

The elliptical contours around the pump axis are in good agreement between the measurement and the simulation. In Fig. 4(b), it can be seen that the maximum displacement due to thermal expansion does not occur at the axis of the pump beam ($x = y = 0$), but is shifted by about 100 μm along the N_m–axis. Figure 4(c) and (d) show the cross section of the height profile at the position of the peak (along the dotted black lines). In 4(c) it can be seen that the surface bulging is not symmetrical around the pump axis. The asymmetry arises from the low symmetry of Yb:KYW, namely the thermal expansion matrix is not diagonal in the eigenframe of the refractive index ellipsoid. The third principal axis of thermal expansion and the z– (N_g–) axis are not parallel and form an angle of about 31° [6]. Therefore, the preferred axis of thermal expansion is tilted with respect to the eigenframe of the refractive index ellipsoid. This explains the shape observed in Fig. 4(c). Meanwhile, because the y– (N_p–) axis coincides with the corresponding

Optical Materials EXPRESS

axis of the thermal expansion eigenframe, no strong asymmetry is visible in Fig. 4(d) for both simulation and measurement. The systematic deviation in the $y<0$ region may result from the pump displaced from the crystal center in the xy–plane, leading to uneven cooling of the crystal.

3.3. Introduced aberrations

The surface bulging shown in Fig. 4 introduces a phase shift that depends on the distance of a given ray from the optical axis. The lowest order contribution that affects the profile of the transmitted beam is a quadratic change in phase along the radial coordinates that acts as a lens. Higher order contributions introduce aberrations. For the Yb:KYW crystal, the non-isotropic crystal properties, including thermal conductivity κ and thermal expansion α_T is a dominant cause of the aberrations. However, the aberrations can also be caused by asymmetric cooling geometry: for example, the cooling is not rotationally symmetric under the geometry given in Fig. 2.

In order to investigate the aberrations of the thermal lens that are introduced purely by the non-isotropic crystal properties, we simulated a rotationally symmetric cooling geometry with a cylindrical rod of radius $R = 2.5$ mm, length $L = 1$ mm, a pump radius $w_P = 150$ µm and absorbed pump power of 6.1 W, wrapped by 1 mm thick indium layer (see Fig. 5). In this setup, the angle dependent aberrations, i.e. tilt, astigmatism and coma, are purely caused by the crystal properties, not by asymmetric cooling. The height displacement of the front surface where the pump beam enters was fitted with the Zernike polynomials $Z_n^m(\rho,\theta)$ representing the primary aberrations [21], where $\rho = r/w_P$ and θ are the (normalized) polar coordinates. The Zernike polynomials $Z_n^m(\rho,\theta)$ are a complete and orthogonal set of functions on the domain $\rho \leq 1$. They are a product of a radial part $R_n^m(\rho)$ and an angular part with angular frequency m. The first eleven polynomials $(n,m) = (0,0),(1,\pm1),(2,0),(2,\pm2),(3,\pm1),(3,\pm3)$ and $(4,0)$ are used in the fit. The fit was performed over a circular disk centered at $x = y = 0$ with a radius given by the pump beam radius w_P. Using the Zernike coefficients $c_{(n,m)}$, the magnitude of the wavefront aberration coefficients W representing piston, tilt, focus, astigmatism, coma, and spherical aberration can be expressed as follows [21]:

$$\begin{aligned}
W_{00} &= c_{(0,0)} - c_{(2,0)} + c_{(4,0)} && \text{piston,}\\
W_{11} &= \sqrt{(c_{(1,1)} - 2c_{(3,1)})^2 + (c_{(1,-1)} - 2c_{(3,-1)})^2} && \text{tilt,}\\
W_{20} &= 2c_{(2,0)} - 6c_{(4,0)} - \sqrt{c_{(2,2)}^2 + c_{(2,-2)}^2} && \text{focus,}\\
W_{22} &= 2\sqrt{c_{(2,2)}^2 + c_{(2,-2)}^2} && \text{astigmatism,}\\
W_{31} &= 3\sqrt{c_{(3,1)}^2 + c_{(3,-1)}^2} && \text{coma,}\\
W_{40} &= 6c_{(4,0)} && \text{spherical aberration.}
\end{aligned} \tag{9}$$

We assume that the phasefront of a beam propagating through the surface described by the set of Zernike coefficients $c_{(n,m)}$ is deformed according to the surface shape. This means that we assume that wavefront aberration is proportional to surface deformation. Using these aberration coefficients the wavefront of a beam passing through the considered surface can be approximated [21]

$$W(\rho,\theta) = W_{00} + W_{11}\rho\cos\theta + W_{20}\rho^2 + W_{22}\rho^2\cos^2\theta + W_{31}\rho^3\cos\theta + W_{40}\rho^4. \tag{10}$$

As an example of a crystal with cubic symmetry, the surface bulging of Yb:YAG is described in the same way. We assumed a thermal conductivity of 4.8 $\mathrm{Wm^{-1}K^{-1}}$ [17] at 50 °C for 10% at. Yb-doping. The fractional heat load and the effective absorption coefficient are taken to be the same as in the simulation for Yb:KYW. Figure 6(a,b) shows the magnitude of the Zernike

Optical Materials EXPRESS

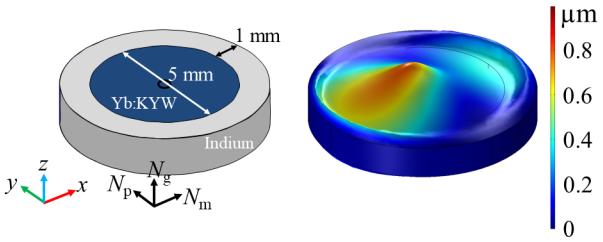

Fig. 5. 3D view of the simulated crystal geometry that was used to obtain the data in sections 3.3 and 3.4. Left: crystal without pump beam. Right: crystal with heating by the pump beam. The pump beam propagates along the z–axis. The colors show the absolute value of the displacement vector. The displacement of the crystal surfaces is exaggerated by a factor of 1500. The deformation visible on the outer part of the cylinder is caused by the radial pressure of the expanding crystal on the soft indium, which bulges outwards as a result. The thin black line that is visible in the right panel is the line that separates the Yb:KYW and the indium without pumping. The radial expansion of the crystal, which compresses the indium, is also responsible for the fact that the separation line between crystal and indium shifts in the pumped case and therefore no longer coincides with the thin black line shown in the figure. In the simulation, the outer surface of the indium layer is kept at a constant position and temperature.

coefficients of the front surface of Yb:KYW and Yb:YAG crystals. It can be seen that the height displacement of the front surface of the Yb:KYW crystal includes a larger contribution from the first and higher order Zernike polynomials while only three coefficients ($(0,0)$, $(2,0)$ and $(4,0)$) are relevant for Yb:YAG. The wavefront aberration coefficients W are shown in Fig. 6(c). While the Yb:YAG crystal exhibits only focus and spherical aberration, contributions of tilt, astigmatism and coma are significant for Yb:KYW due to asymmetric thermal expansion. The dioptric power of the surface bulging contribution of the thermal lens in the Yb:YAG crystal is smaller by a factor of 5-6 compared to Yb:KYW. The investigation shows that the thermal lensing due to surface bulging is much stronger in Yb:KYW for a given absorbed power.

For Yb:KYW, since $c_{(2,2)}$ (astigmatism along the x– and y–axes) is much larger than $c_{(2,-2)}$ (astigmatism along lines expressed by $x = y$ and $x = -y$), the sagittal and meridional planes of the lens are approximately aligned along the xz– (mg–) and yz– (pg–) planes, respectively. The combined focusing power of the front and back surfaces of the crystal results in focal lengths of $f = 105$ mm and $f = 118$ mm, respectively for mg– and pg–planes, giving a normalized difference of 11%. The tilt represented by W_{11} deflects the transmitted beam. As an example, when a laser beam at wavelength of $\lambda = 1045$ nm focused to $w = 150$ µm passes through the front surface of the crystal, the deflection angle introduced by the tilt is 15% of the divergence half angle of the laser beam. The effect can be avoided by setting the propagation axis parallel to one of the eigenvectors of the thermal expansion matrix. For example the crystal can be cut such that $\vec{k} \parallel N_p$. This is the only axis that is an eigenvector of the thermal expansion matrix and a principal axis of the refractive index. If the attenuation of the pump beam at the crystal is small, the back and front surfaces of the crystal will receive comparable amounts of heating from the pump beam. This is also the case when the pump beam is backfolded or two-sided pumping is used. The front and back faces will have the same shape, but will be rotated 180 degrees around the pg–plane. The $c_{(n,m)}$ coefficients for both surfaces are comparable in magnitude, but have opposite signs for even n. Therefore, the odd aberrations (tilt and coma) introduced by the front and back surfaces cancel each other out, while the even aberrations (focus, astigmatism, and spherical aberration) add up.

Optical Materials EXPRESS

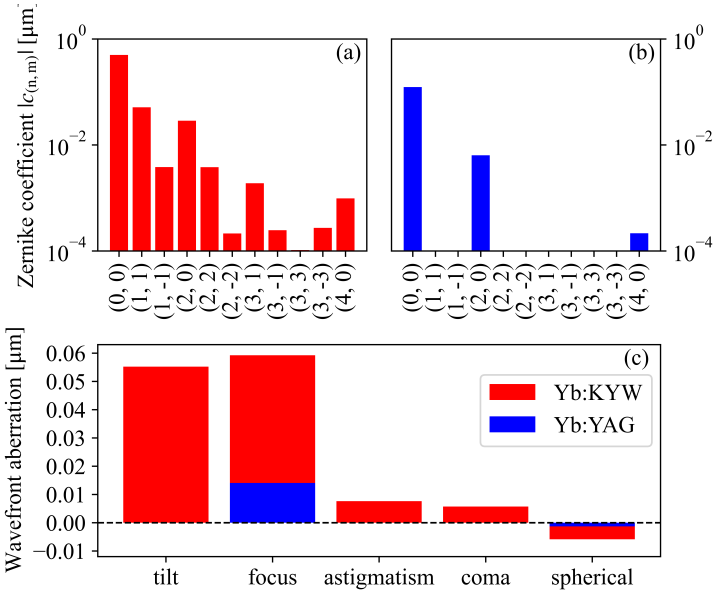

Fig. 6. The magnitude of the Zernike coefficients extracted from the simulated height profile of the front surface (where the pump beam enters) of (a) Yb:KYW and (b) Yb:YAG crystals. The pump radius used in the simulation is 150 μm. The incident pump power is set to 10 W and the absorption coefficient of $\alpha = 937$ m^{-1} is used. The absorbed power is 6.1 W. (c) Wavefront aberration coefficients derived from the Zernike coefficients (see Eq. (9) for the definitions).

When a long or highly doped Yb:KYW crystal is used, the attenuation of the pump beam at the crystal is significant and the deflection of the beam introduced by W_{11} at the front and back surfaces does not cancel. The effect is expected to be significant, for example, in the setup reported in [22], where a $3 \times 3 \times 3$ mm crystal with 5% doping was used with pump average power of 10 W and a radius of $w_P = 50$ μm. While the surface bulging induced beam displacement is small (1.3% compared to the pump radius), the deflection angle amounts to 19% of the laser divergence angle. In the setup used in [7], a crystal with the dimensions $1.2(N_m) \times 6.0(N_p) \times 3.0(N_g)$ mm was pumped at $\lambda = 981$ nm pump radiation. The pump radius of $w_P = 175$μm and a maximum power of 25 W were employed. The absorbed pump power reaches 19 W. According to our numerical simulation, the deflection angle is even 37% of the laser divergence angle. When the crystal is installed in the laser cavity, this effect can lead to a pump power-dependent misalignment of the cavity. Some laser geometries with a monolithic cavity (e.g. microchip lasers) may require pre-compensation of this effect in the cavity design. Undoped endcaps at both ends of the gain medium may suppress the surface bulging [11,18].

The astigmatic thermal lens has been reported in Yb:KYW solid state oscillator [7]. In this work, by measuring the intracavity beam profile, it was found that the dioptric power of the overall thermal lens on the Yb:KYW crystal for rays in the *mg*–plane is about 21-35% (depending on the polarization) larger than that of the *pg*–plane. The authors of [7] attribute the astigmatism to the photoelastic contribution (χ_{PE}), assuming that the surface bulging contribution (χ_{bulg}) is symmetric. According to our simulation performed under the experimental conditions given in [7], χ_{bulg} was found to be 5.3 and 4.8×10^{-6} K^{-1} for the *mg*– and *pg*–planes, respectively, and exhibits an astigmatism of about 10%. Therefore our investigation suggests that about a third of the astigmatism is caused by surface bulging and the rest is due to the photoelastic contribution (χ_{PE}), which confirms that the photoelastic effect is not the only source of astigmatic thermal

Optical Materials EXPRESS

lensing in Yb:KYW, and stigmatic surface bulging is not a good approximation. It should be noted that the bulging coefficient χ_{bulg} obtained from our simulation is inconsistent with the simple model of $\chi_{\mathrm{bulg}} = (n-1)\alpha_{\mathrm{T}}$, which gives $\chi_{\mathrm{bulg}} = 17.8 \times 10^{-6}$ K^{-1} and 16.9×10^{-6} K^{-1} for laser polarization of $E \parallel N_{\mathrm{m}}$ and $E \parallel N_{\mathrm{p}}$, respectively [7]. The model assumes non-astigmatic surface bulging under a large aspect ratio of $w_{\mathrm{P}}^{*} = 2w_{\mathrm{P}}/L$ and cannot be applied to the Yb:KYW crystal in the setup described in [7] (see discussion in the following section).

3.4. Surface bulging effect for different pump radius

In sec. 2, it is discussed that the expression $\chi_{\mathrm{bulg}} = (n_0 - 1)(1 + \nu)\alpha_{\mathrm{T}}$ holds only if there is no stress along the axial direction ($\sigma_z = 0$), i.e. the entire crystal length contributes to thermal expansion. If only a fraction of the crystal length contributes to expansion, the bulging coefficient can be modeled by Eq. (5), where it was assumed that the fraction of the crystal length that contributes to thermal expansion can be parametrized by the aspect ratio $w_{\mathrm{P}}^{*} = 2w_{\mathrm{P}}/L$. Although such simple modeling is only applicable to an isotropic medium where the thermal conductivity κ and the thermal expansion coefficient α_{T} reduce to scalar values, it would still be interesting to investigate the pump radius dependencies of χ_{bulg} for Yb:KYW crystals.

We assume that Eq. (5) can still be valid by using an effective scalar value of the thermal expansion coefficient $\alpha_{\mathrm{T}}^{\mathrm{eff}}$. We expect that this effective thermal expansion coefficient $\alpha_{\mathrm{T}}^{\mathrm{eff}}$ is dependent on the thermal expansion matrix α_{T}, the pump propagation direction and the details of the cooling geometry, and to have possibly two different values for the meridional and sagittal planes reflecting astigmatism. It is not known how to calculate $\alpha_{\mathrm{T}}^{\mathrm{eff}}$ from the entries of the thermal expansion matrix α_{T}, it can only be determined indirectly via experimental or numerical evaluation of χ_{bulg}. In [23], $\alpha_{\mathrm{T}}^{\mathrm{eff}} = \alpha_{\mathrm{T},zz}$ was assumed where z is the pump propagation axis. We expect that this assumption is not valid for Yb:KYW, because we have confirmed that the off-diagonal entries of α_{T} play an important role in thermal lensing due to surface bulging, as discussed in sections 3.1 and 3.3. Instead we evaluated χ_{bulg} for different aspect ratios $w_{\mathrm{P}}^{*} = 2w_{\mathrm{P}}/L$. The simulation was repeated for different pump radii w_{P} while keeping the incident and absorbed pump power constant at $P_{\mathrm{abs}} = 6$ W. The resulting wavefront deformation was fitted with Zernike polynomials and the dioptric power of the thermal lens due to surface bulging is calculated according to Eq. (9). While the full anisotropic thermal conducivity was used throughout the numerical simulations, Eq. (6) is only valid for materials with isotropic thermal conductivity. Therefore we employ the average thermal conductivity $\langle\kappa\rangle = 3.3$ Wm^{-1}K^{-1} for conversion from dioptric power to bulging coefficient χ_{bulg} according to Eq. (6). We extracted χ_{bulg} for different pump radii. The results are shown in Fig. 7.

In the regime where the aspect ratio $w_{\mathrm{P}}^{*}<1$, we observe that χ_{bulg} decreases as the aspect ratio approaches zero. However, we found that a power law $\chi_{\mathrm{bulg}} = (n_0 - 1)\alpha_{\mathrm{T}}^{\mathrm{eff}}(w_{\mathrm{P}}^{*})^{\gamma}$ describes the surface bulging contribution where $w_{\mathrm{P}}^{*}<1$ more accurately than a linear dependence on the aspect ratio (Eq. (5)). We fit our simulation results with this power law using the exponent γ as a free parameter. A γ in the range of 0.5 to 0.6 best reproduces the simulation results. In the simulation, the temperature dependence of α_{T} was neglected. Elevated medium temperature may increase the effective thermal expansion coefficient ($\alpha_{\mathrm{T}}^{\mathrm{eff}}$) and results in smaller γ. Using the temperature dependence of the N_{g} component of the thermal expansion coefficient given in [20], we expect that the change in $\alpha_{\mathrm{T}}^{\mathrm{eff}}$ due to the temperature rise is at most 10% under typical design of amplifiers and lasers where the temperature increase of the Yb:KYW crystal is kept well below 100 °C.

For larger aspect ratio ($w_{\mathrm{P}}^{*}>1$) we found that the values approach $\chi_{\mathrm{bulg},\infty} = 20.7$ and 18.4×10^{-6} K^{-1} for the *mg*– and *pg*–planes, respectively. Our numerical results confirm that the crossover between the two different models for χ_{bulg} is at $w_{\mathrm{P}}^{*} = 1$. The astigmatism caused by the surface bulging is about 11%. We confirmed that the extracted $\chi_{\mathrm{bulg},\infty}$ is weakly dependent on the pump power by running the simulations for absorbed pump power ranging from 6 W to

Optical Materials EXPRESS

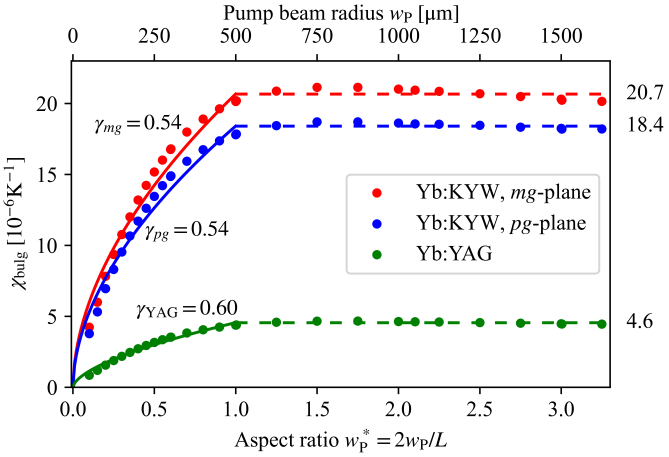

Fig. 7. The bulging coefficient χ_{bulg} is evaluated by numerically simulating the surface bulging for Yb:KYW and Yb:YAG crystals. The simulation was repeated for different pump radii w_P (top x–axis). The crystal length (in propagation direction) of L = 1 mm and absorbed pump power of P_{abs} = 6.1 W were used for all simulations. While the full anisotropic thermal conducivity was used throughout the numerical simulations, Eq. (6) is only valid for materials with isotropic thermal conductivity. Therefore we employ the average thermal conductivity $\langle\kappa\rangle$ = 3.3 Wm^{-1}K^{-1} for conversion from dioptric power to bulging coefficient χ_{bulg} according to Eq. (6). Red and blue dots correspond to χ_{bulg} for the mg– and pg–planes, respectively. The bottom x–axis is given by the aspect ratio $w_P^* = 2w_P/L$ where w_P. At high aspect ratios, the simulation data shows a constant value given by the horizontal red, blue, and green dashed lines corresponding to $\chi_{bulg,\infty}$ = 20.7, 18.4, and 4.6×10^{-6} K^{-1} for the Yb:KYW mg–/pg–planes and Yb:YAG, respectively. These are the average values of χ_{bulg} shown in this plot for the aspect ratio larger than unity. The solid lines are best fit by a power law given by $\chi_{bulg}/\chi_{bulg,\infty} = (w_P^*)^\gamma$, where the exponent γ is left as a fitting parameter. The fit was performed for the aspect ratio ranging from 0 to 1.0. It was found that γ lies in a range from 0.5 to 0.6 to best reproduce the numerical data.

12 W. This is consistent the linear dependence of the thermal lens dioptric power on the pump intensity given in (6). The obtained bulging coefficients at large aspect ratio limit ($\chi_{bulg,\infty}$) agree with the values reported in [7] within 14% and 19% respectively for laser polarization of $E \parallel N_m$ and $E \parallel N_p$. Yumashev and co-authors [23] made analytical calculations for stress and strain under the plane stress approximation and derived the "effective Poisson ratio" ν^*, which leads to the result $\chi_{bulg} = (n_0 - 1)(1 + \nu^*)\alpha_T$ = 19.1 and 18.7×10^{-6} K^{-1} for the sagittal and meridional planes, respectively. Our results for $\chi_{bulg,\infty}$ agree with the values calculated in [23] within 8% and –2%, respectively.

For comparison, we simulated the same setup with a YAG crystal (green dots and lines in Fig. 7). It can be seen that the value of $\chi_{bulg,\infty}$ is considerably smaller than that of Yb:KYW: ($\chi_{bulg,\infty,YAG} = 4.6 \times 10^{-6}$ K^{-1}). This value is in good agreement with $\chi_{bulg} = (n_0 - 1)\alpha_T = 4.2 \times 10^{-6}$ K^{-1}, assuming $\alpha_T = 5.1 \times 10^{-6}$ at 50 °C [17], and n = 1.82 [8], confirming that the model is applicable to symmetric crystals like Yb:YAG.

For KYW, as w_P is further increased and the ratio of pump radius to rod radius w_P/R approaches 1, χ_{bulg} begins to increase (see Fig. 8). At w_P/R = 1, we obtained χ_{bulg} = 22.9 and 22.7×10^{-6} K^{-1}, for mg– and pg–plane, respectively. The difference between the two planes reduced to 1%. We believe this is because the region of expansion extends close to the clamped surfaces and the isotropic pressure of the clamping weakens the anisotropy of the thermal expansion. The small difference between the meridional and the sagittal plane agrees

Optical Materials EXPRESS

with the results from Ref. [23], where 2% difference is reported. However, the magnitude of their results is about 17% smaller than ours. One possible explanation for the discrepancy is our definition of dioptric power, which subtracts the effect of spherical aberration (see Eq. (9)), whereas the model by [23] ignores aberrations. The regime where w_P/R approaches 1 is not very realistic experimentally because a significant fraction of the pump beam does not fit to the crystal.

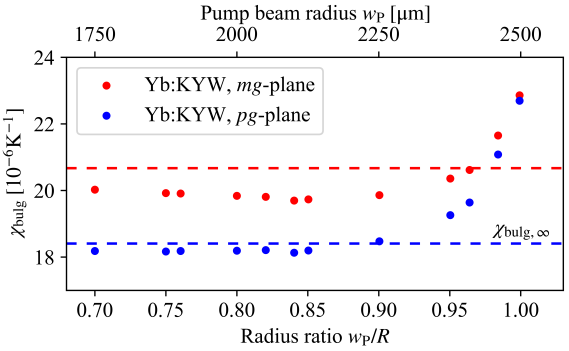

Fig. 8. The bulging coefficient χ_{bulg} is evaluated by numerically simulating the surface bulging of Yb:KYW crystals with even larger pump beam radius (w_P) than shown in fig. 7. Other simulation parameters are identical to those used in fig. 7. The horizontal axis is given by radius ratio w_P/R, where R = 2.5 mm is the radius of the rod. The dashed lines indicate $\chi_{bulg,\infty}$ given in fig. 7. Note that even close to homogeneous heating (i.e. $w_P/R \rightarrow 1$) surface bulging occurs, because the temperature profile is not constant due to the boundary condition that the external surface of the indium layer is kept at a constant temperature.

4. Conclusion and outlook

We have measured surface bulging in an end-pumped Yb:KYW crystal and compared the surface profile with numerical simulations using material parameters including elasticity matrix, thermal conductivity and thermal expansion matrix. While the surface bulging is known to introduce astigmatic thermal lensing [12], we found that the effect in Yb:KYW is more significant than previous studies indicate [7,23]. In particular, in the investigated setup, the bulging contribution of the thermal lens has an astigmatism of 10%. This implies that 30% of the overall astigmatism of the thermal lens are caused only by the bulging effect. Previously, such astigmatism was underestimated [23] or ignored [7] by simple theoretical modeling of surface deformation. Furthermore we found that in KYW the surface bulging contribution of the thermal lens can cause beam deflection and displacement. The similar numerical simulation of surface bulging can also be applied to other gain materials and different pump geometries, proving a useful method for estimating surface bulging-induced thermal lensing, especially when the material exhibits anisotropic thermal expansion and simple analytical modeling cannot be applied. Our numerical results should qualitatively agree with the bulging effect of other monoclinic crystals, such as Yb:KGW or Yb:KLuW. For isotropic crystals, simple analytical modeling may offer a sufficiently accurate estimation.

For a more complete description of thermal lensing it is also necessary to include contributions from the thermo-optic coefficient χ_T and the photoelastic coefficient χ_{PE}. The numerical evaluation of these parameters is sometimes not straightforward because low-symmetry materials have a large set of unknown material constants that are required to evaluate these coefficients: For example in order to evaluate χ_T, the quantity $(\partial n/\partial T)_{\vec{\varepsilon}}$ must be obtained experimentally. The elasto-optic tensor of Yb:KYW has to be known precisely to evaluate χ_{PE}. For materials with monoclinic crystal structure, the elasto-optic tensor has 20 independent entries, of which only

Optical Materials EXPRESS

12 have been measured so far for Yb:KYW [24]. A reliable evaluation of the surface bulging contribution using our numerical method would improve the accuracy when estimating χ_T and χ_{PE} by subtracting the surface bulging contribution from the experimental measurement of the total thermal lensing effect.

Funding. European Research Council (742247); Deutsche Forschungsgemeinschaft (EXC-2111 – 390814868).

Acknowledgments. This work was funded by the Deutsche Forschungsgemeinschaft (DFG, German Research Foundation) under Germany's Excellence Strategy – EXC-2111 – 390814868 and the European Research Council (ERC) under the European Union's Horizon 2020 research and innovation programme (grant agreement No. 742247).

Disclosures. The authors declare no conflicts of interest.

Data availability. Data underlying the results presented in this paper are not publicly available at this time but may be obtained from the authors upon reasonable request.

References

1. L. M. Osterink and J. D. Foster, "Thermal effects and transverse mode control in a Nd:YAG laser," Appl. Phys. Lett. **12**(4), 128–131 (1968).
2. P. Russbueldt, T. Mans, G. Rotarius, *et al.*, "400 W Yb:YAG Innoslab fs-amplifier," Opt. Express **17**(15), 12230–12245 (2009).
3. P. Russbueldt, D. Hoffmann, M. Höfer, *et al.*, "Innoslab amplifiers," IEEE J. Sel. Top. Quantum Electron. **21**(1), 447–463 (2015).
4. U. Brauch, A. Giesen, M. Karszewski, *et al.*, "Multiwatt diode-pumped Yb:YAG thin disk laser continuously tunable between 1018 and 1053 nm," Opt. Lett. **20**(7), 713–715 (1995).
5. J. E. Hellström, S. Bjurshagen, V. Pasiskevicius, *et al.*, "Efficient Yb:KGW lasers end-pumped by high-power diode bars," Appl. Phys. B **83**(2), 235–239 (2006).
6. P. Loiko, K. Yumashev, N. Kuleshov, *et al.*, "Detailed characterization of thermal expansion tensor in monoclinic K*Re*$(WO_4)_2$, where *Re*=Gd, Y, Lu, Yb," Opt. Mater. **34**(1), 23–26 (2011).
7. P. Loiko, S. Manjooran, K. Yumashev, *et al.*, "Polarization anisotropy of thermal lens in Yb:KY$(WO_4)_2$ laser crystal under high-power diode pumping," Appl. Opt. **56**(10), 2937–2945 (2017).
8. W. Koechner, "Thermal Lensing in a Nd:YAG Laser Rod," Appl. Opt. **9**(11), 2548–2553 (1970).
9. S. Chénais, F. Druon, S. Forget, *et al.*, "On thermal effects in solid-state lasers: The case of ytterbium-doped materials," Prog. Quantum Electron. **30**(4), 89–153 (2006).
10. W. A. Clarkson, "Thermal effects and their mitigation in end-pumped solid-state lasers," J. Phys. D: Appl. Phys. **34**(16), 2381–2395 (2001).
11. M. Kilinc, U. Demirbas, J. B. Gonzalez-Diaz, *et al.*, "Thermal and population lensing of Yb:YLF at cryogenic temperature," Opt. Mater. Express **13**(11), 3200–3216 (2023).
12. K. V. Yumashev and P. A. Loiko, "Thermal stresses and end-bulging in the laser disc from a tetragonal [100]-cut crystal," Laser Phys. **25**(1), 015003 (2015).
13. P. A. Loiko, K. V. Yumashev, N. V. Kuleshov, *et al.*, "Thermo-optical properties of pure and Yb-doped monoclinic KY$(WO_4)_2$ crystals," Appl. Phys. B **106**(3), 663–668 (2012).
14. I. V. Mochalov, "Laser and nonlinear properties of the potassium gadolinium tungstate laser crystal KGd$(WO_4)_2$:Nd^{3+}-(KGW:Nd)," Opt. Eng. **36**(6), 1660–1669 (1997).
15. M. Mazur, D. Velikovskiy, L. Mazur, *et al.*, "Elastic and photo-elastic characteristics of laser crystals potassium rare-earth tungstates K*RE*$(WO_4)_2$, where *RE*=Y, Yb, Gd and Lu," Ultrasonics **54**(5), 1311–1317 (2014).
16. P. A. Loiko, K. V. Yumashev, V. N. Matrosov, *et al.*, "Dispersion and anisotropy of thermo-optic coefficients in tetragonal $GdVO_4$ and YVO_4 laser host crystals," Appl. Opt. **52**(4), 698–705 (2013).
17. X. Xu, Z. Zhao, J. Xu, *et al.*, "Thermal diffusivity, conductivity and expansion of $Yb_3xY_{3(1-x)}Al_5O_{12}$ ($x = 0.05$, 0.1 and 0.25) single crystals," Solid State Commun. **130**(8), 529–532 (2004).
18. R. Weber, B. Neuenschwander, M. Mac Donald, *et al.*, "Cooling schemes for longitudinally diode laser-pumped Nd:YAG rods," IEEE J. Quantum Electron. **34**(6), 1046–1053 (1998).
19. COMSOL Multiphysics v. 6.2. www.comsol.com. COMSOL AB, Stockholm, Sweden.
20. K. V. Yumashev, E. E. Trusova, S. A. Guretskii, *et al.*, "Thermal expansion of monoclinic $KYb_xY_{1-x}(WO_4)_2$ laser crystals," Appl. Phys. B **130**(1), 14 (2024).
21. J. C. Wyant and K. Creath, "Basic wavefront aberration theory for optical metrology," Applied Optics and Optical Engineering **11**, 28–39 (1992).
22. G. H. Kim, G. H. Yang, D. S. Lee, *et al.*, "High-power efficient cw and pulsed lasers based on bulk Yb:KYW crystals with end diode pumping," Quantum Electron. **42**(4), 292–297 (2012).
23. K. Yumashev and P. Loiko, "Thermal stress and end-bulging in monoclinic crystals: the case study of double tungstates," Appl. Opt. **56**(13), 3857–3866 (2017).
24. M. Mazur, L. Mazur, and V. Pozhar, "Specific directions of ultrasound propagation in double potassium tungstates for light modulation," Ultrasonics **73**, 231–235 (2017).